HOSTED BY
ELSEVIER
Available online at www.sciencedirect.com
ScienceDirect
Soils and Foundations 63 (2023) 101330
SOILS AND FOUNDATIONS
www.elsevier.com/locate/sandf

Technical Paper

Insights on the role of local site effects on damage distribution in the Izmir metropolitan area induced by the October 30, 2020 Samos earthquake

Anna Chiaradonna [a,*], Eyyub Karakan [b], Cem Kincal [c,d], Giuseppe Lanzo [e], Paola Monaco [a], Alper Sezer [f], Mourad Karray [g]

[a] *University of L'Aquila, P. le Pontieri 1, Monteluco di Roio, 67100 L'Aquila, Italy*
[b] *Kilis 7 Aralik Universitesi, Mehmet Sanlı Street, 79000 Kilis Merkez, Kilis, Türkiye*
[c] *Dokuz Eylul University, Engineering Faculty, Geological Engineering Dept. Tinaztepe Campus, Buca, İzmir, Türkiye*
[d] *Dokuz Eylul University, The Graduate School of Natural and Applied Sciences, Tinaztepe Campus, Buca, İzmir, Türkiye*
[e] *Sapienza University of Rome, via Antonio Gramsci, 53, Rome 00197, Italy*
[f] *Ege Universitesi, İnşaat Mühendisliği Bölümü, 35040 Bornova, İzmir, Türkiye*
[g] *Université de Sherbrooke, 2500, boul. de l'Université J1K 2R1, Canada*

Received 9 January 2023; received in revised form 11 May 2023; accepted 26 May 2023

Abstract

On the 30th of October 2020, a 6.6 magnitude earthquake occurred 14 km north of Samos Island, causing 119 casualties (117 in Izmir, Türkiye, and 2 in Samos, Greece) and significant damage in the 3rd biggest city of Türkiye, Izmir. Although the city is roughly 70 km far away from the epicenter, the damage was significant and concentrated in the city center settled on alluviums. This paper aims to analyze the distribution of damage in Izmir province, by crosschecking the recorded motions, the subsoil conditions and the evidence of damage as collected by an *ad-hoc* on-site reconnaissance. The intrinsic behavior of the Samos earthquake was investigated by employing three different ground-motion prediction equations. The results of the analyses revealed that site effects play a significant role in the amplification of ground motions, and valley effects are responsible for the concentration of damage. The damage in buildings was classified in terms of the intensity and structural typologies for the 30 districts of Izmir metropolitan area. In-depth analysis of the distribution of damages revealed that the earthquake caused damage all over the boundaries of Izmir province, and the concentration of damage in Bornova and Karşıyaka districts has a clear correlation with double resonance effects.

Keywords: 2020 Samos Earthquake; Damage distribution; Site effects; Earthquake records; Ground motion parameters; GMPE model; Basin effects; Double resonance

1. Introduction

On October 30, 2020, a damaging earthquake of moment magnitude 6.6 struck approximately 14 km northeast of the island of Samos, Greece, and approximately 70 km from the center of the city of Izmir in Türkiye (AFAD, 2020). The rupture occurred on a previously mapped normal fault, referred to as the North Samos Fault or the Kaystrios Fault, in the Aegean Sea (Fig. 1a). This earthquake is the first event with a magnitude greater than 6.0, which occurred to the south of the city of Izmir since 1977 (AFAD, 2020). The mainshock was recorded at

Peer review under responsibility of The Japanese Geotechnical Society.
* Corresponding author.
E-mail address: anna.chiaradonna1@univaq.it (A. Chiaradonna).

https://doi.org/10.1016/j.sandf.2023.101330
0038-0806/

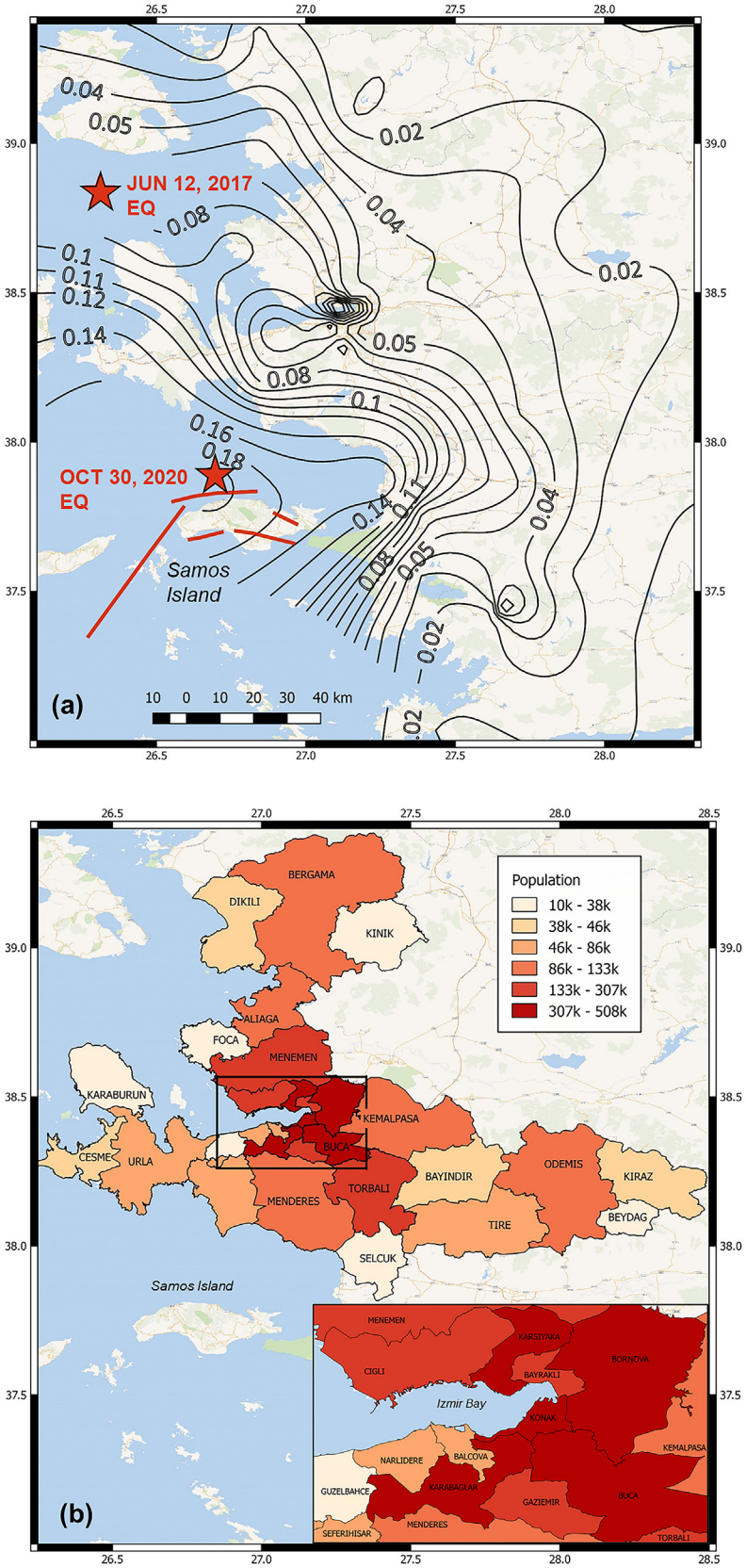

Fig. 1. Map showing the epicenter of 30th October 2020, fault lines around Samos region and contours of peak ground acceleration (PGA) in western Türkiye. Also reported in the figure is a) epicenter of 12th June 2017 earthquake; b) distribution of the population among the districts of the Izmir metropolitan area.

several seismic stations in the Turkish strong-motion network. Fig. 1a presents the peak ground acceleration (largest of the two horizontal components) contours based on 160 records obtained from the Turkish seismic network (AFAD, 2020), showing that the recorded motion between 60 and 70 km distance from the epicenter of the earthquake is generally in the range 0.02—0.14 g.

Izmir is the third largest city in the country according to the number of inhabitants (about 4 million) and incorporates the second largest port in Türkiye. Composed of 30 districts (Fig. 1b), the population is concentrated around the Inner Bay, where the majority of the damage was observed. Geologically, this part is covered by alluvial soils bounded by E-W trending active normal faults in the stretching Aegean Province. Young alluvium (Holocene) and the fan delta with shallow marine deposits are confined and controlled by the Izmir fault to the south, and the KFZ-Karşıyaka Fault Zone to the north constitutes the thickest sediments in the basin (Fig. 2b). The basin fill exceeds 300 m in thickness in the middle part of the Bornova Plain (Pamuk et al., 2017).

Although the epicenter was not close, the effects of the seismic event were destructive in the city center, resulting in 117 casualties, over 1030 injuries, and more than 5000 people homeless, who were temporarily housed in tents, and a hotel that was partially managed by Izmir metropolitan municipality.

The Ministry of Environment, Urbanisation and Climate Change (2020) reported that out of a total of 1,810 schools, 517 mosques, and 1,919 public buildings, 18 schools, 10 mosques, and 20 public buildings were heavily damaged while 33 schools, 18 mosques, and 23 public buildings were moderately damaged.

In contrast, despite the short distance from the epicenter, limited damage was observed on the Greek island of Samos, where only two fatalities and 19 minor injuries were reported.

Izmir and its periphery are surrounded by more than 20 active fault zones, which may trigger one another's activity (Moberg, 2015). Large earthquakes have been experienced in the past centuries, especially between 1600 and 1800 CE. It is worth mentioning nine events with reported Modified Mercalli Intensity (MMI) higher than 8 (e.g., Ambraseys, 2009). The earthquakes of 1668, 1739, 1778, 1880, and 1883 CE, with MMI ≅ 9, had epicenters along the coastal part of the Aegean Sea. During the instrumental period (after 1926), Izmir and its periphery experienced five significant earthquakes. In chronological order: 1928 (M = 6.5)

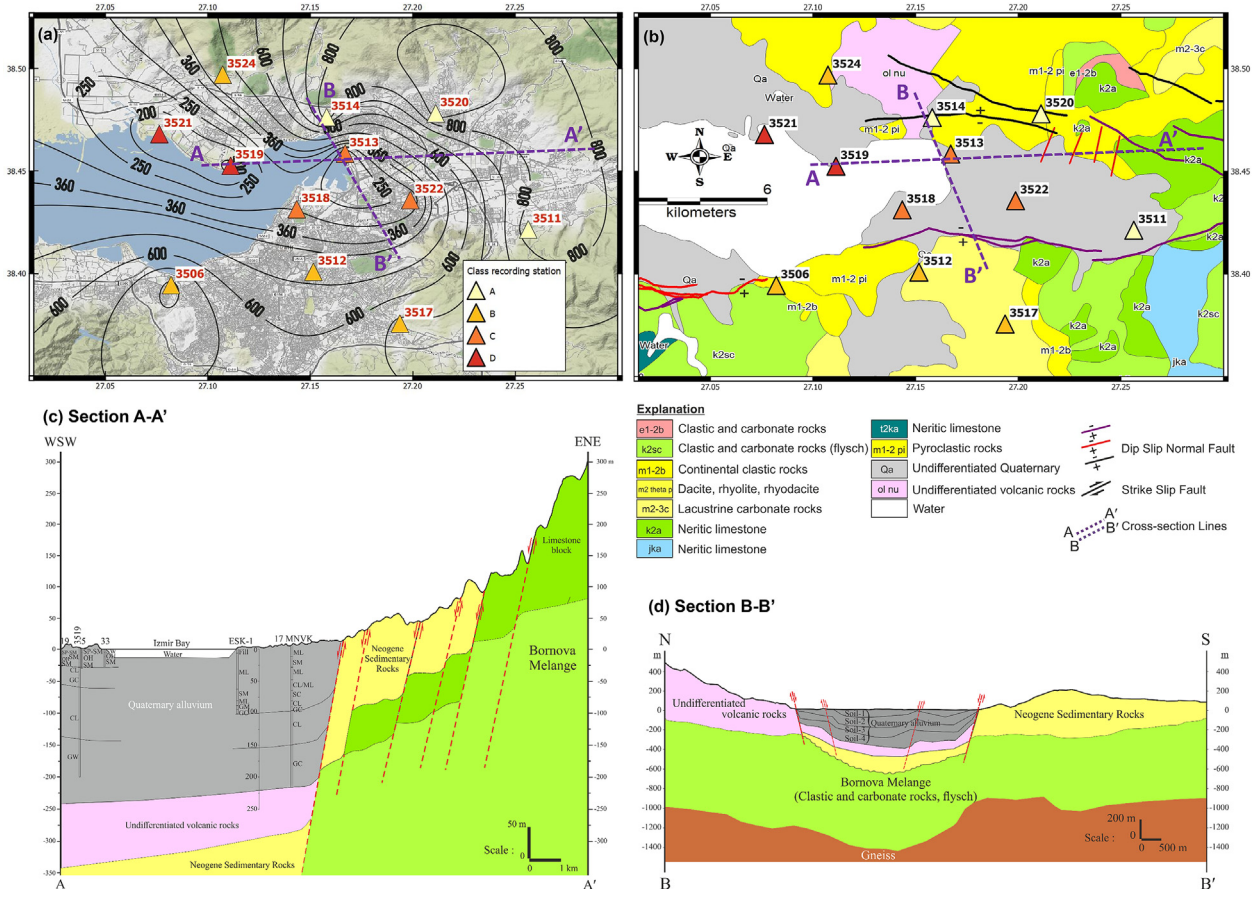

Fig. 2. a) Distribution of the recording stations in the Izmir region and contours of equivalent shear wave velocity, $v_{S,30}$ (m/s) obtained from the subsoil classification of the recording stations; b) Geological map of the Izmir Bay (Akbaş et al., 2011) with the trace of the cross-sections A-A′ and B-B′, c) Geological cross-section A- A′, and d) Geological cross-section B- B′ (modified after Kıncal (2005) and Pamuk et al. (2017)).

Torbalı, 1949 (M = 6.6) Karaburun, 1992 (M = 6.0) Doğanbey, 2003 (M = 5.7) Seferihisar and 2005 (M = 5.4 – 5.8) Sığacık events (Çetin et al., 2020). Owing to the high seismicity, many studies were performed to map the ground shaking and liquefaction susceptibility of the region (Sezer et al., 2008; Guillier et al., 2008; Altun et al., 2012).

More recently, several studies (Akinci et al., 2021; Makra et al., 2021; Nuhoglu et al., 2021) compared the seismic parameters measured in the Izmir area after the October 2020 earthquake, where significant damage was observed, along with a short evaluation of the 1975, 1998, 2007 and 2019 Turkish Earthquake code provisions for design spectra. As reported by Makra et al. (2021) and Erdik et al. (2020), most of the heavily damaged structures were built before 1990 and were probably designed using the oldest code (1975). According to Yakut et al. (2021), a remarkable portion of damaged buildings seems to be constructed during 1990–2000, while the structural damages in the buildings constructed after 2010 were markedly low.

The comparison between the design spectra (1975 or later) with those of the recorded signals made it possible to understand the extent of the damage (Makra et al., 2020; 2021; Nuhoglu et al., 2021). However, this comparison does not explain the entire observed damage since the October 30, 2020 event does not correspond to the worst scenario expected by the code (Yakut et al., 2021), neither in terms of magnitude nor distance. The related spectra are therefore covered by the seismic provisions of the building codes (TSDC 2007; TBEC 2018). Yakut et al. (2021) attributed the main reason for damage to a significant lack of code compliance, by describing the presence of soft stories, lack of proper detailing, poor construction quality, and of heavy over- hangs, as revealed during visual inspections of the survey teams.

Cetin et al. (2022) reported that soil amplifications are more pronounced in the spectral period range of 0.5–1.5 s. Also, they observed that these amplified periods coincide with the natural period of 7–9 story, reinforced concrete buildings. However, the analyses in this study can be extended by a systematical and accurate analysis of the damage, particularly concerning the spatial distribution and intensity of the observed damage through the different construction typologies of the built environment.

In this regard, this study aims to provide insights into the role of local site effects with an in-depth analysis of the damage in the Izmir metropolitan area, based on a careful collection and data analysis of both seismic records and damage observations. In the following sections, a review of basin effects observed after far-field shakings is recalled, and similarities and differences are highlighted compared to the geological and seismological assets in the Izmir region. The main features of the October 30, 2020 mainshock, including a critical discussion about the intensity of the motion recorded and related predictions provided by the most suitable ground motion prediction equations are reported. In addition, detailed analyses of the recorded motions in Izmir Bay are provided and overlapped with the conditions of the local subsoil to identify local site effects (basin effects, local stratigraphic amplification, and so on). An overall assessment of damage distribution is performed by a field survey, which considers the characteristics of the built environments (type and number of stories) furtherly integrated with data obtained from the Ministry of Environment, Urbanisation and Climate Change. Possible interrelationships between damage distribution and site effects are comparatively investigated to assess the main reasons for the loss of lives and property, and critically discussed. The lessons learned and open issues to be addressed in future studies are summarized in the concluding section.

2. Brief review of observed basin effects

During many past and recent earthquakes, it has been commonly observed that the presence of valleys/basins leads to much more complex amplification phenomena (e.g., basin effects) than those typical of simple 1D conditions. Particularly, there are several well-documented examples of basins located at moderate to large distances from the epicenter, where such effects were observed. The first example is the response of the Caracas Valley during the 1967 earthquake that caused severe damage to multistorey buildings, although the magnitude was only 6.4 and its epicenter was located approximately 60 km from Caracas (Seed et al., 1972). The most significant feature of the damage pattern was the concentration of the damage in specific locations (Palos Grandes district) and on certain types of structures (i.e., 10 to 12 storey apartment buildings), while damage to low structures in the same district was relatively minor. Papageorgiou and Kim (1991) analyzed the propagation and amplification of seismic SH waves in the Caracas Valley using 1D and 2D models. They found that the predicted 2D amplification ratios were consistent with the damage distribution that occurred during the 1967 earthquake, whereas the 1D model predicted deamplification in the same areas. Another paradigmatic example is the 1985 Michoacan earthquake (M_w = 8.0) which hit Mexico City, causing more than 350 buildings to collapse and almost 20,000 casualties (Garini et al., 2020), nearly 350 km away from the epicenter. It damaged only a part of the city, and mainly 8- to 17-storey buildings collapsed (Resendiz and Roesset, 1986). The significant long-period amplification and long shaking duration were generally attributed to basin-edge effects, reverberation, and amplification of seismic waves within the sedimentary and highly plastic clay deposits (Seed et al., 1988), which also led to an extended duration of seismic signals. Several other similar cases can be cited: the strong and prolonged ground motion observed in the La Molina sediment-filled basin in Lima during the 1974 Peru earthquake (Stephenson et al., 2009), the level of damage experienced in the city of Kirovakan and Leninakan, which are built

on sedimentary valleys, following the 1988 Armenia (M = 6.8) earthquake (Yegian et al., 1994; Bielak et al., 1999), and the basin-edge effects occurred in the Marina district during the October 1989 Loma Prieta earthquake (M = 7.1) (Graves, 1993; Zhang and Papageorgiou, 1996). Recently, Kaikōura earthquake (M = 7.8) struck the Wellington region of New Zealand, located 60 km north of the uppermost fault rupture (Bradley et al., 2018). Despite the relatively large distance from the epicenter, amplification of long-period ground motions due to impedance contrast and basin edge effects in the Thorndon and Te Aro basins in Central Wellington resulted in appreciable ground motion and subsequent damage to the built environment; in particular, in some locations, spectral accelerations exceeded the 500-year return period design ground motion levels between 1 and 2 s (McGann et al., 2021). Interestingly, similar amplification effects in the Wellington region were also observed for the moderate intensity ground motion during the two earthquakes in 2013: Cook Strait (M = 6.6) and Lake Grassmere (M = 6.6) earthquakes, whose epicenters were 50 km and 70 km away from the Wellington region, respectively (Holden et al., 2013). All these examples remind the effects of the 2020 Samos event on Izmir city center (Bayraklı district and its periphery), where the distance from the epicenter was approximately 70–75 km.

3. Geology of Izmir and its environment

Damage after the event was concentrated in Bornova Plain. On average, this plain (in fact, basin) is approximately 13 km long and 7 km wide (Fig. 2b). Two representative geological cross-sections, named A-A′ (Fig. 2c) and B-B′ (Fig. 2d), having WSW-ENE and N-S direction, respectively, show the basin of the Bornova Plain.

The region has characteristics common to many basins worldwide, such as the presence of active faults bordering the plain and morphology that can induce 2D or 3D effects (Fig. 2b,c,d). The Late Cretaceous formations in the vicinity of Izmir consist of sandstone, shale, and limestone blocks. Generally, these formations outcrop at the peaks circumscribing the area. Basic units belonging to the Aegean region are shown in Fig. 2b and related parameters, as investigated by Pamuk et al. (2017), are reported in Table 1. The average of S-wave velocities shows that the Bornova Mélange rocks reflect the features of the bedrock in the north and south part of the study area (Pamuk et al., 2018).

Streams cause the accumulation of alluvial sediments in the Bornova Plain. The geological units depicted above are discordantly overlain by alluvium. Alluvial plains around Izmir Bay have different geomorphological characteristics. Partially, the eastern and northern shorelines of the city is established on alluvial delta plains (Kayan, 2000). The most damaged area, the Bornova Plain, is constrained by Izmir Bay and is a sedimentary basin surrounded by the Nif and Yamanlar mountains. Mixtures of clay, silt, sand, loam, and fill are encountered in the topsoil profile, where the mechanical properties are quite poor, as reported in Table 1. Alluvial soils were also classified into four different soil layers (Soil-1, Soil-2, Soil-3 and Soil-4 in Fig. 2d) as reported in Pamuk et al. (2017).

Kincal (2005) presented Standard Penetration Tests (SPT) performed in 422 boreholes in the study area. It was observed that the SPT blow count values vary between 0 and 50. Especially on the waterfront, these values are less than 20 and increase as we proceed to the east (Fig. 2b). It is particularly important to notice the remarkable contrast of stiffness between the rocks and the alluvial sediments (Table 1), which contributes to the amplification of the ground motion at the surface.

A concave structure was detected by several researchers (Kıncal, 2005; Pamuk et al., 2017; Pamuk et al., 2018), as reported in Fig. 2d. The depth of the bedrock (V_S greater than 760 m/s) changes from 150 to 450 m in the Bornova Plain and is approximately 450 m at the coastline (Pamuk et al., 2018).

As a consequence, the predominant period values of the basin vary between 0.45 and 1.6 s where the regions have thick soil layers from rivers in the Bornova Plain, and decrease gradually from the bay (Pamuk et al., 2019).

The Department of the Earthquake of the Ministry of Interior of the Turkish government installed a dense seismograph array (16 seismic stations in the bay and a total of 36 in Izmir Province). Many of the seismic stations in the vicinity of Izmir province were established after 2010, while several were established in 2007. This network successfully recorded strong ground motions during the events produced in the last decade. Fig. 2 presents the distribution of the seismic stations in the Izmir region (Fig. 2a), overlapped on the contours of equivalent shear wave velocity, $V_{S,30}$ obtained from the subsoil classification of the recording stations based on EC8 (CEN 2004).

4. Salient features of ground motion parameters of October 30, 2020 earthquake

The October 30, 2020 earthquake occurred at 13:51 UTC on the northern coasts of Samos Island, at coordinates (37.9001°N, 26.8057°E) and a focal depth of 12 km according to the Institute of Geodynamics, National Observatory of Athens (NOAIG). The peak ground acceleration (PGA) recorded on soft rock was approximately 0.173 g at the closest station located in Samos Prefecture (Greece), 19 km from the epicenter (Kalogeras et al., 2021).

Table 2 provides the observed ground motion characteristics recorded by the stations located around Izmir Bay (Fig. 2a) along with the station number, equivalent shear wave velocity in the first 30 m, $V_{S,30}$, site class according to Eurocode 8 code (CEN 2004), and source-to-site distance. As shown in Fig. 1, the Peak Ground Acceleration (PGA) of the recorded motion at a distance of 70 km from the epicenter is very low, and the peak ground acceleration on the rock subsoil (class A) around the Izmir city center is

Table 1
Descriptive parameters for soil and rock (modified after Pamuk et al., 2017).

Soil/Rock Types	Average V_S (m/s)	Thickness (m)
Quaternary alluvium Soil-1: Clay, Silt clay	200	15–120
Quaternary alluvium Soil-2: Clay, Sandy gravel	600	30–110
Quaternary alluvium Soil-3: Clay, Gravelly clay	400	40–100
Quaternary alluvium Soil-4: Clayey gravel, Clay-claystone	650	60–150
Undifferentiated volcanic rocks (outcropped)	860	300–400
Neogene sedimentary rocks (outcropped)	770	100–350
Undifferentiated volcanic rocks and Neogene sedimentary rocks (embedded)	1200	100–300
Bornova Melange (Clastic and carbonate rocks, flysch)	2000	600–850
Gneiss	>3000	–

Table 2
Characteristics of seismic recordings of October 30, 2020 earthquake, by the stations around Izmir Bay.

Station number	$V_{S,30}$ (m/s); Subsoil class	R (km)	PGA (g)	S_a [T = 0.3 s] (g)	S_a [T = 1 s] (g)	S_a [T = 3 s] (g)
3520	875 (A)	75.8	0.060	0.088	0.112	0.010
3514	836 (A)	73.4	0.057	0.100	0.123	0.008
3511	827 (A)	72.6	0.042	0.083	0.070	0.009
3506	771 (B)	62.3	0.042	0.121	0.043	0.007
3517	695 (B)	65.3	0.041	0.093	0.051	0.011
3512	468 (B)	65.8	0.059	0.179	0.082	0.008
3524	459 (B)	73.6	0.070	0.202	0.074	0.008
3523	414 (B)	48.9	0.082	0.213	0.067	0.016
3513	196 (C)	72.0	0.108	0.286	0.347	0.031
3518	298 (C)	68.3	0.108	0.261	0.195	0.019
3519	131 (D)	69.2	0.153	0.249	0.468	0.041
3521	145 (D)	69.6	0.113	0.214	0.205	0.055

generally less than 0.06 g (Table 2). Conversely, the stations located on thick alluvial deposits in the center of the valley indicate PGAs that reach 0.15 g around station 3519 and 0.11 g at station 3521 (Chiaradonna et al., 2022b).

The intensity of the shaking was compared with the estimate provided by existing Ground-Motion Prediction Equations (GMPEs). The use of the GMPEs aims to quantify the variations of ground motions from the south direction from which the seismic wave propagated up to the Izmir metropolitan region. In this study, three empirical models were used (Table 3) according to Boore and Atkinson (2008), Akkar and Çağnan (2010), and Akkar and Brommer (2010), hereafter referred to as BA08, AÇ10, and AB10.

In Fig. 3, the recorded peak ground acceleration (PGA) and spectral accelerations (S_a) for selected periods (T = 0.3 s, T = 1 s, and T = 3 s) at distances of up to 400 km (green symbols) are compared with the three selected GMPEs, for a rock site ($V_{S,30}$ greater than 800 m/s) and normal faulting type (black lines).

The observed PGA and selected spectral accelerations were fairly consistent with the values predicted by the AB10 and BA08 models. Conversely, the AÇ10 model, developed explicitly for Türkiye, underestimates the PGA and the spectral acceleration (S_a) at T = 0.3 s, whereas it well predicts the spectral acceleration at periods higher than 1 s.

The observation of the data in the region of Izmir Bay (between 60 and 80 km) reveals that the seismic parameters

Table 3
Adopted GMPE models.

Model	Abbreviation	Region	No. records, No. main shocks	M_{min}-M_{max}	Distance (km)
Boore and Atkinson (2008)	BA08	Worldwide	1574, 58	5—8	0—400
Akkar and Çağnan (2010)	AÇ10	Türkiye	1259, 573	3.5—7.6	0—200
Akkar and Brommer (2010)	AB10	European Mediterranean	532, 131	5.0—7.6	0—200

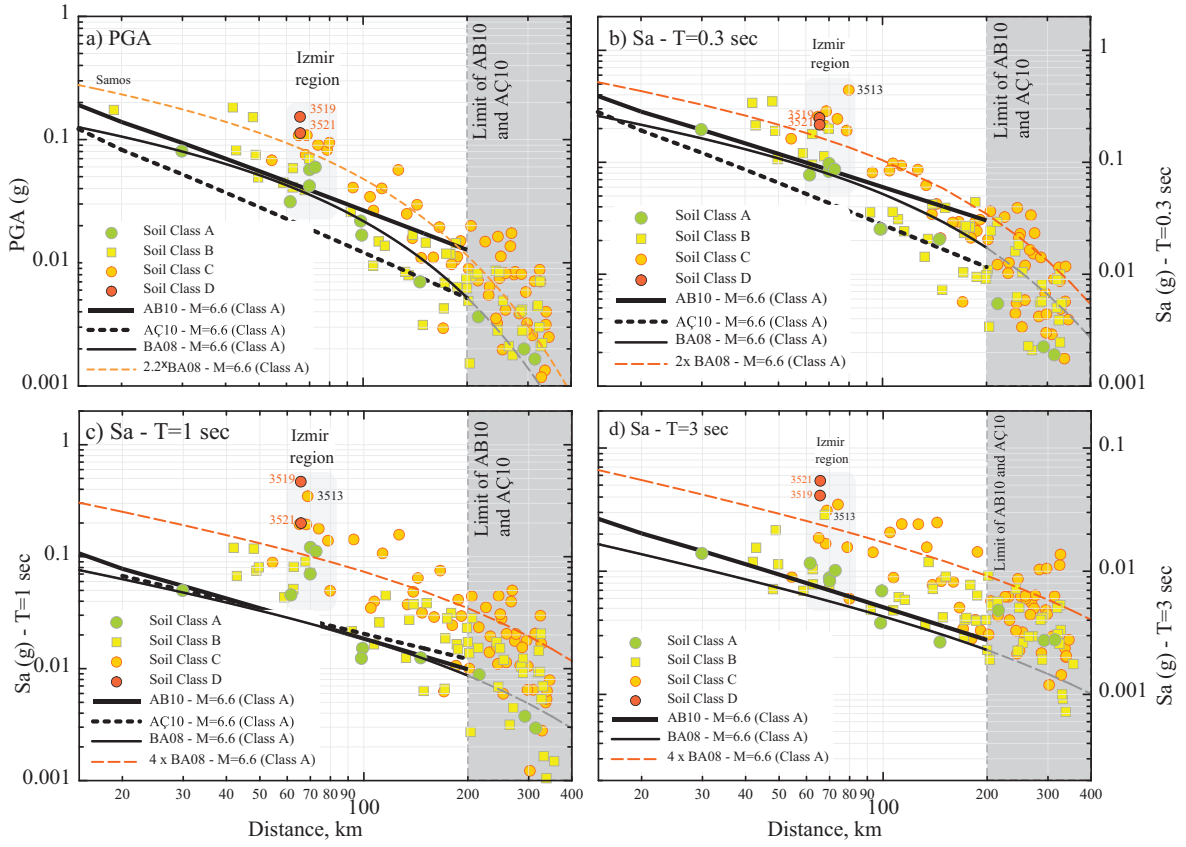

Fig. 3. Comparisons of a) PGA, b) S_a (T = 0.3 s), c) S_a (T = 1 s) and d) S_a (T = 3 s) measured on soil Class A from the 30 October 2020 earthquake with AB10, AÇ10 and BA08 GMPEs models computed for a rock site ($V_{S,30}$ greater than 800 m/s) and normal faulting type. Data from class B, class C and class D (yellow, orange and red symbols, respectively) are also shown and compared with GMPE proposed by Boore and Atkinson (2008) multiplied by an amplification factor..

are generally higher than those of the models proposed for Türkiye. This is particularly true for the spectral acceleration at period T = 1 s, which is the closest value to the fundamental period of the alluvial deposit in the Bornova valley (Makra et al., 2021; Pamuk et al., 2019).

Additionally, data from recording stations settled on sites classified as subsoil class B, C and D are shown in Fig. 3 and compared with GMPE proposed by Boore and Atkinson (2008) multiplied by an amplification factor (red dotted lines).

Out of 160 station records, only 119 were considered for which $V_{S,30}$ was available. As shown in Fig. 3, the majority of the data refer to site categories B (56) and C (50), whereas limited data are available for D (2) site classes.

The amplification factors obtained globally (10 to 300 km) between class C soil and class A (excluding the Izmir Bay region) according to BA08 GMPE model are of the order of 2.2 for PGA (Fig. 3a), 2 for S_a at a period of 0.3 s (Fig. 3b) and 4 for S_a at periods of 1 s and 3 s (Fig. 3c and 3d).

The response spectra of the recorded signals by stations installed on the rock (class A) in Izmir periphery (Chiaradonna et al., 2022a) are compared in Fig. 4a with those calculated from the GMPEs proposed by Boore and Atkinson (2008) and Akkar and Brommer (2010). The GMPE model by Akkar and Çağnan (2010) was not used in this comparison because it underestimated the measured values. Fig. 4a shows that the records from the Izmir region are richer in terms of energy at lower frequencies (larger periods). The spectra show very little variation in spectral acceleration along a wide period band (plateau between 0.25 s and 1.5 s), which is fundamentally different from the spectra established by GMPEs where spectral acceleration decreases with increasing periods.

Fig. 4b shows a comparison between the spectra obtained from the recorded signals on soil class B and AB10 and BA08 models. The GMPEs better reproduced the recorded signals for soil class B than for soil class A. In contrast, the comparison with the signals recorded on class C soil (Fig. 4c) and class D soil (Fig. 4d) shows significant differences and highlights the presence of the same plateau observed in the signals recorded on class A soil between 0.25 s and 1.5 s. The amplification factor of the spectral acceleration between 0.25 s and 1.5 s is about 2.5 for soil class C and 3 for soil class D.

The comparisons highlight important differences in terms of frequency content between the GMPEs and the recorded signals in the region of Izmir Bay. This difference

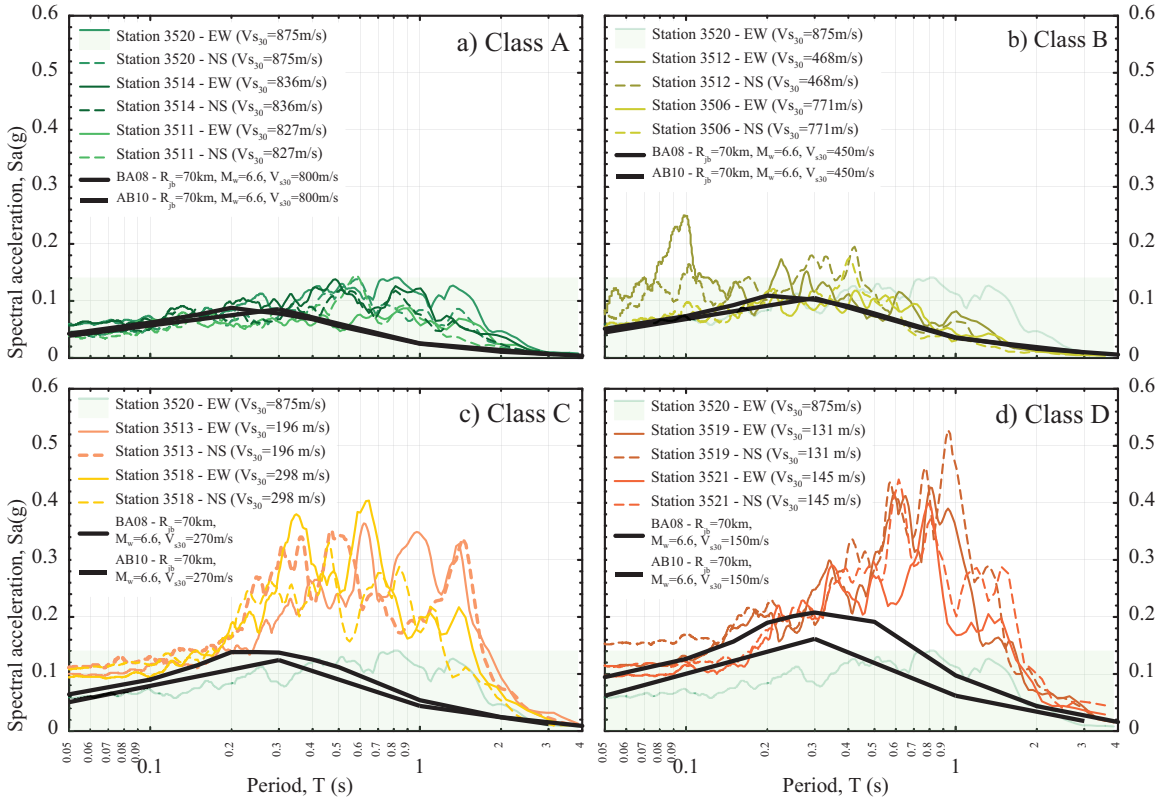

Fig. 4. Acceleration response spectra of the two horizontal component motions east–west and north–south) registered during the Samos earthquake by different stations installed around Izmir Bay on different classes of soil: a) Class A, b) Class B, c) Class C, and d) Class D, compared with the predictions provided by the considered GMPEs.

is probably the result of local geology in the Izmir region, as noted by Pamuk et al. (2019). As stated by Gulerce et al. (2022), differences in the median estimation of GMPEs from the observed ground motions may be related to several factors such as source effects, site amplification effects or inconsistencies in the depth, magnitude and distance scaling among others. In particular, the available empirical equations are not well constrained at large distances in basin configurations due to the scarcity of suitable empirical data. It is difficult to isolate the different effects with limited data from one earthquake only. However, for this specific earthquake, the source factor and the basin effects appear to be important contributors to the enhanced long-period motions recorded in Izmir area (Cetin et al., 2021; Gulerce et al., 2022).

Therefore, it is relevant to analyze signals recorded during a seismic event whose source comes from another direction. Indeed, Fig. 5 presents a comparison between the response spectra of the recorded signals during the June 12, 2017 earthquake, located 20.73 km north-west of Karaburun and about 84 km from Izmir Bay (Fig. 1a), at the same stations installed on class A soil around Izmir bay and the spectra determined using BA08 and AB10 GMPEs. Fig. 5 shows that the BA08 and AB10 GMPEs predict the response spectra fairly well for periods larger than 0.3 s which is not the case for records measured during the October 30, 2020 earthquake.

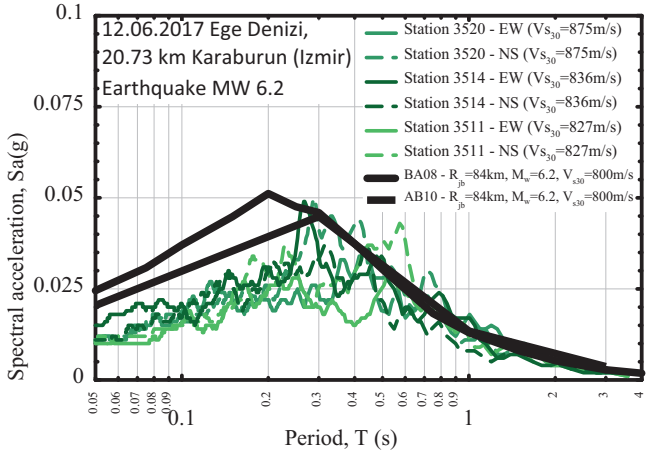

Fig. 5. Acceleration response spectra of the two horizontal components east–west and north–south) of the motion registered during the 12th June 2017 Karaburun earthquake by different class A stations installed around Izmir Bay.

While amplitude and frequency content variations were highlighted in the previous figures, the elongation of the duration of the shaking inside the basin was indirectly investigated through the Arias Intensity, which is the time-integral of the square of the ground acceleration (Arias, 1970). Fig. 6 reports the trend (best-fit line) of the Arias intensity, calculated for the recorded signals in the

range of the Joyner-Boore distance, R_{jb}, between 62.5 and 79 km, as a function of $V_{S,30}$ of the correspondent recording stations. Moving from class A to class D (decreasing of $V_{S,30}$), the calculated Arias intensity shows a marked increase. The main districts of Izmir Bay are also reported to circumscribe the basin and identify the valley effect (subsoil class C and D).

5. Description and assessment of damages

5.1. Description of observed damage

Building stock in Izmir is composed of several types of structures that can be classified into three categories: reinforced concrete buildings with six stories or more, reinforced concrete buildings with less than six stories, and masonry buildings with one to two stories. These structures were built during different periods and designed following different codes, i.e., 1975, 1998, 2007, and 2018. After the earthquake on October 30, 2020, teams employed by the Ministry of Environment, Urbanisation and Climate Change performed a comprehensive reconnaissance study throughout Izmir Province. Moreover, an independent on-site reconnaissance after the earthquake was made by a team supported by some of the authors. According to the Ministry of Environment, Urbanisation and Climate Change (2020), damage in buildings can be classified into low, moderate, and heavy damage by simple observations. Slightly damaged buildings were distinguished by slender cracks and fissures in the building plaster, walls, and paint caused by ground shaking. These observations lead to the fact that the buildings are still operational. Moderately damaged buildings were defined by discontinuities in frames and slender cracks on load-bearing elements. Building use is not permitted until the damaged elements are reinforced or repaired. Heavily damaged buildings showed wide shear cracks and cleavages in the load-bearing elements of the structure, which cannot be reverted to their initial performance by reinforcement and maintenance. Fig. 7 presents examples of typical damages observed after the earthquake. Inappropriate superstructural design and field application, low-quality of concrete and reinforcement detailing, under-designed beam-column joints, formation of soft stories, and short columns were more frequently observed (Cetin et al., 2021; Demirci et al., 2021; Akansel and Özkula, 2021, Yakut et al., 2021). The information obtained was used to classify the damage that occurred, by methodologies proposed by Boduroglu et al. (2013) and modified by Ilki et al. (2020).

5.2. Damage distributions

In Fig. 8, the number of different-levels damaged buildings in the districts in Izmir Province is presented along with contours of Arias Intensity (AI). The AI values are maximized in the Bayraklı, Bornova, and Karşıyaka districts where the damage is concentrated, and the valley effect is also much more pronounced. In this respect, irrespective of the level of damage, the maximum number of slightly, moderately, and heavily damaged buildings were determined to be within the boundaries of Bayraklı, Bornova, and Karşıyaka districts.

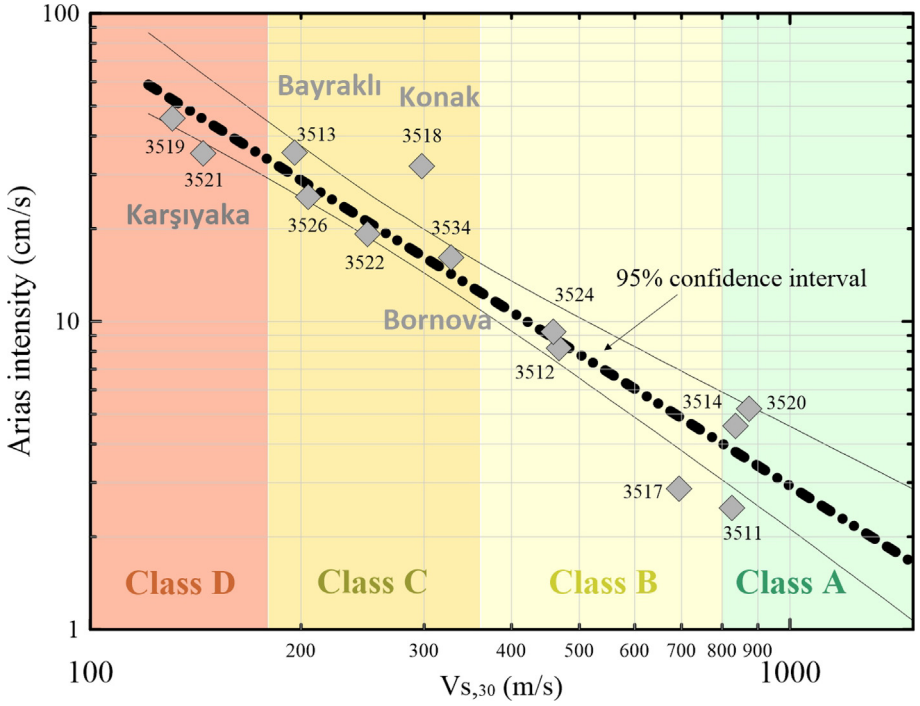

Fig. 6. Arias intensity vs. $V_{S,30}$ in the region of Izmir Bay.

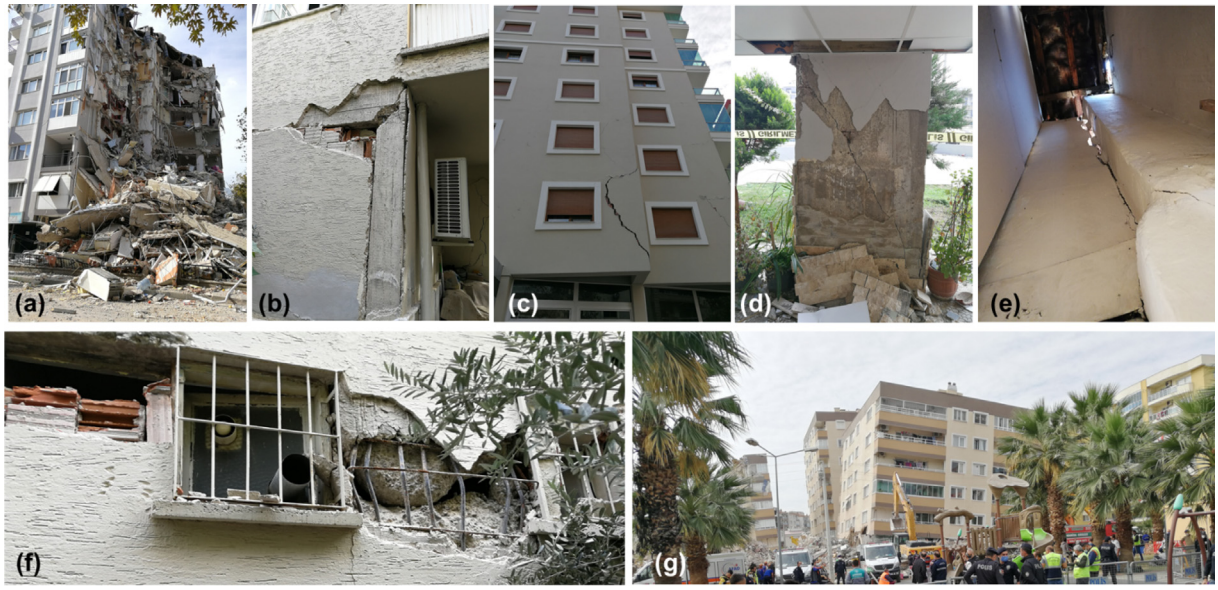

Fig. 7. (a) Partially collapsed building in Manavkuyu District (heavy damage) (b) Failure of the beam-column joint (moderate damage) (c) Formation of cracks (moderate damage) (d) Damage due to soft story effects in Karşıyaka (heavy damage) (e) Relative movements in a masonry building in Konak District (heavy damage) (f) Short column formation (moderate damage) (g) Building with first floor collapse (heavy damage).

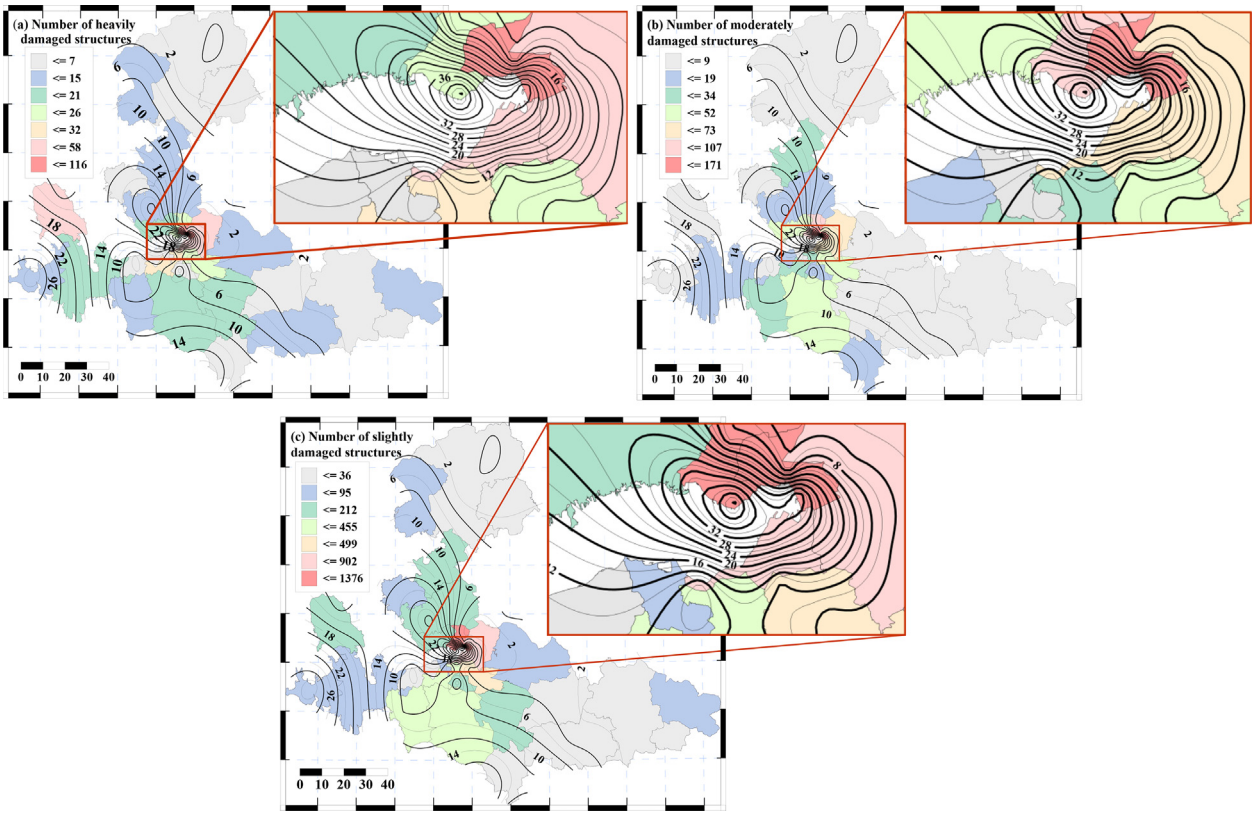

Fig. 8. The number of a) heavily, b) moderately and c) slightly damaged structures in inhabited areas of Izmir metropolitan municipality correlated with contours of Arias intensity (in cm/s).

The AI values are consistent with the number of damaged buildings in the coastal districts of Izmir, which are close to the epicenter of the earthquake. Karaburun, Çeşme, Urla, and Seferihisar among these districts, were also affected by the occurrence of the tsunami. However, the number of stories of buildings in these districts is quite low in comparison with those located in a highly residential city center, which was another reason for the lower number

of damaged structures. As expected, damage levels are lower in northern and eastern districts (Dikili, Bergama Kınık, Bayındır, Kemalpaşa, Ödemiş, Beydağ and Tire), which are underpopulated in comparison with districts constituting the city center (Fig. 8).

Table 4 presents the number and level of damage for the most damaged districts, while the damage in the remaining districts is recorded as "Other." Structural damage is concentrated in Bayraklı and Bornova districts, while damage in the Karşıyaka district is also significant. Near collapsed buildings, older buildings of three to five stories survived after the ground shaking and suffered only slight damage. According to the Ministry of Environment, Urbanisation and Climate Change (2020), 50 buildings collapsed in Izmir, compared to the total number of buildings, which is more than 158,000. This value may seem to be very low concerning the total number of buildings; however, it represents an anomaly when compared to other sites with the same distance and the same PGA/S_a (T) from the epicenter, where damage was not observed.

Thirty-five buildings were urgently leveled, while the numbers of slightly, moderately, and heavily damaged buildings were 6683, 688, and 581, respectively. These numbers normalized to the total number of buildings (ratios in Table 4) reveal that different levels of damage are concentrated in the Bornova and Bayraklı districts, followed by the Karşıyaka district (Fig. 8a). Menderes and Seferihisar districts are closer to the epicenter of the Samos earthquake and, despite the tsunami that occurred after the earthquake, the number of damaged buildings and their damage ratios were lower. Damages were observed in Kiraz, which is the most distant district from the epicenter in the east direction (Fig. 8a, 1b). The same observations can be made in Dikili, Bergama, and Kinik districts, which are far from the epicenter and located to the north. However, the ratio of collapsed buildings is comparably high in Bayraklı and Bornova districts, because these districts are highly residential and populated, and the number of casualties was higher. The number of moderately damaged buildings in Bayraklı (3.00‰) and Karşıyaka (1.85‰) districts were the highest, and Bornova had a ratio of 1.27‰. Slightly damaged buildings in Bayraklı (24.22‰) or Karşıyaka (21.87‰) districts are greater than the sum of those in the remaining 20 districts, labeled as "Other" in Table 4 (20.96‰). Karşıyaka, Bayraklı, and Bornova districts, where the majority of the concentrated building stock is settled on alluvium, were exposed to a greater amount of damage.

A lower amount of damage was observed in districts almost equally close or closer to the epicenter (Urla and Çeşme). This is attributed to the low population and fewer buildings, and the absence of basin effects in these districts. However, these coastal areas were also affected by the earthquake-induced tsunami, so to avoid misinterpretation, data from these districts were not reported in Table 4.

5.3. Damage assessment

Considering the structural features, individual maps based on building type and height were prepared for the most damaged area. In this regard, Fig. 9 shows peak ground acceleration (PGA) and spectral accelerations (S_a) at periods T of 0.3 and 1 s, Arias Intensity (AI), and the distribution of slightly, moderately, and heavily damaged concrete buildings with a number of stories greater than or equal to 6.

Regarding PGA, Karşıyaka district is also subject to a basin effect due to reflections from Yamanlar Mountain, while a slightly lower PGA is observed in Bayraklı district, where damage and collapsed structures are concentrated (Fig. 9a). The analyses reveal that the contours of AI, S_a (T = 0.3 s), and S_a (T = 1 s) are compatible with those of the PGA. Heavy damages for concrete buildings with more than or equal to 6 storey are observed for S_a (T = 1 s) values ranging between 0.20 g and 0.35 g in Karşıyaka, while corresponding values in Bayraklı district are in the range of 0.17 g and 0.25 g. For moderately damaged structures, S_a (T = 1 s) values lie over a very broad range. A similar distribution of S_a (T = 0.3 s) is observed; however, contours covering heavily damaged concrete structures of a number of stories more than 6 range between 0.20 g and 0.26 g in Karşıyaka and between

Table 4
Building stock in Izmir and reported levels of damage (Report of the Ministry of Environment, Urbanisation and Climate Change, 2020).

District	Total number of buildings	Level of damage							
		Collapsed	Ratio (‰)	High	Ratio (‰)	Moderate	Ratio (‰)	Slight	Ratio (‰)
Bornova	56,646	7	0.12	59	1.04	72	1.27	894	15.78
Bayraklı	31,493	9	0.16	127	2.24	170	3.00	1372	24.22
Seferihisar	13,994	2	0.04	23	0.41	33	0.58	235	4.15
Aliağa	14,223	2	0.04	11	0.19	20	0.35	107	1.89
Buca	57,989	1	0.02	28	0.49	49	0.87	428	7.56
Karabağlar	38,379	2	0.04	21	0.37	33	0.58	345	6.09
Karşıyaka	153,743	6	0.11	25	0.44	105	1.85	1239	21.87
Kemalpaşa	2114	0	0	10	0.18	2	0.04	42	0.74
Konak	37,237	3	0.05	40	0.71	55	0.97	642	11.33
Menderes	5896	1	0.02	23	0.41	29	0.51	192	3.39
Other	84,679	17	0.30	214	3.78	120	2.12	1187	20.96

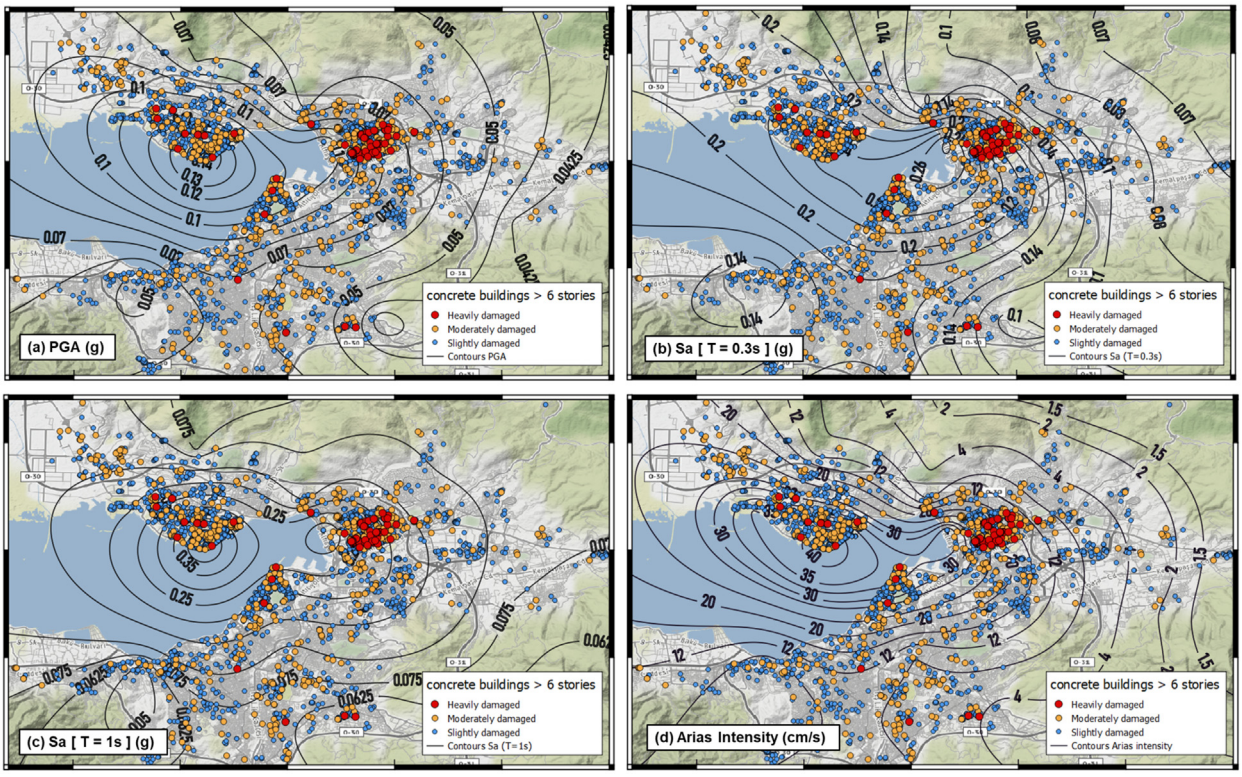

Fig. 9. Distribution of slightly, moderately and heavily damaged concrete buildings with more than 6 stories correlated with the contours of a) PGA, b) S_a (T = 0.3 s), c) S_a (T = 1 s) and d) Arias Intensity.

0.14 g and 0.24 g in Bayraklı and Bornova districts. Moderately damaged structures are accompanied by S_a (T = 0.3 s) values between 0.10 g and 0.14 g. Slight damage can barely be associated with the intensities of PGA, S_a, and AI values.

The damaged buildings are concentrated in a limited area, where the natural period of the structure (0.6 – 1 s) tends to be strongly excited by the amplified shaking in the same range of periods (0.3 – 1 s) (see also Fig. 4c).

For residential structures up to 7–9 stories, Ziotopoulou et al. (2022) reported that foundation systems were mostly identified as two-way combined footings or individual footings with strip beams. Due to the nature of the shallow foundation, inertial soil-structure-interaction effects could have been generated. To evaluate the elongation period of those buildings, the structure-to-soil stiffness ratio has been estimated. According to the NIST (2012), the structure-to-soil stiffness ratio, h/(V_S T), is the ratio between the height of the center of mass for the first mode shape, estimated as 2/3 of the building height, and the product between V_S (the shear wave velocity of the foundation soils) and T (the period of the fixed base structure, i.e., not considering the inertial soil-structure-interaction effects that induced elongation of the period of the structure). According to TBEC (2018), the fixed base period of the 7 to 10 story buildings is ranging from 0.9 to 1.3 s. Assuming an average height of storey of 3 m, and a V_S ranging between 300 and 600 m/s, the structure-to-soil stiffness ratio, h/(V_S T) is less than 0.07 so that the period lengthening due to the inertial soil-structure-interaction can be neglected (NIST 2012).

Consequently, the approximate estimation of the fundamental periods of these high structures is included in the 0.6 – 1.5 s range of periods where the higher spectral accelerations were observed (Fig. 4c). This highlights a double resonance effect among ground motion, soil deposits, and high concrete buildings, which reasonably explains the severe damage suffered by such structures.

Fig. 10 illustrates the same distributions for concrete structures with a number of stories less than 6. Analyzing Fig. 10a, it is noticed that the PGA contours are again good descriptors of heavy and moderate damage; however, the damage distribution throughout Izmir city is more evident. In contrast to Fig. 9, the basin effects are not pronounced as for higher concrete buildings, and the damage distribution is widespread. AI values are as low as 6 and 3 can be associated with heavy and moderate damages for concrete structures with fewer stories than 6, respectively. Slight damage is not dependent on the intensity of the PGA, S_a, and AI values.

Fig. 11 shows the distribution of damage in the masonry buildings in Izmir. In fact, after 1970, owing to high seismic threat, almost all buildings are reinforced concrete structures, while older structures remain to be masonry. Because there is a great need for housing in Izmir, many of the old structures were demolished and these parcels were used to

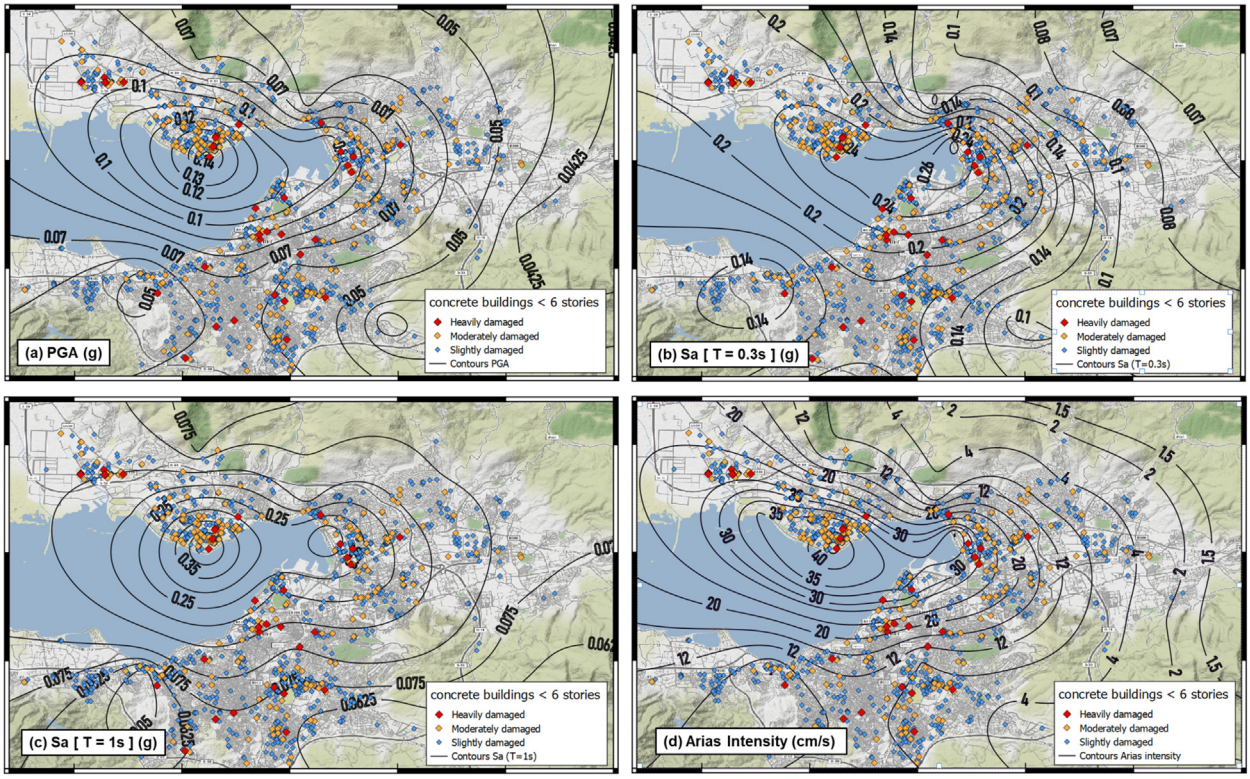

Fig. 10. Distribution of slightly, moderately and heavily damaged concrete buildings with less than 6 stories correlated with the contours of a) PGA, b) S_a (T = 0.3 s), c) S_a (T = 1 s) and d) Arias Intensity.

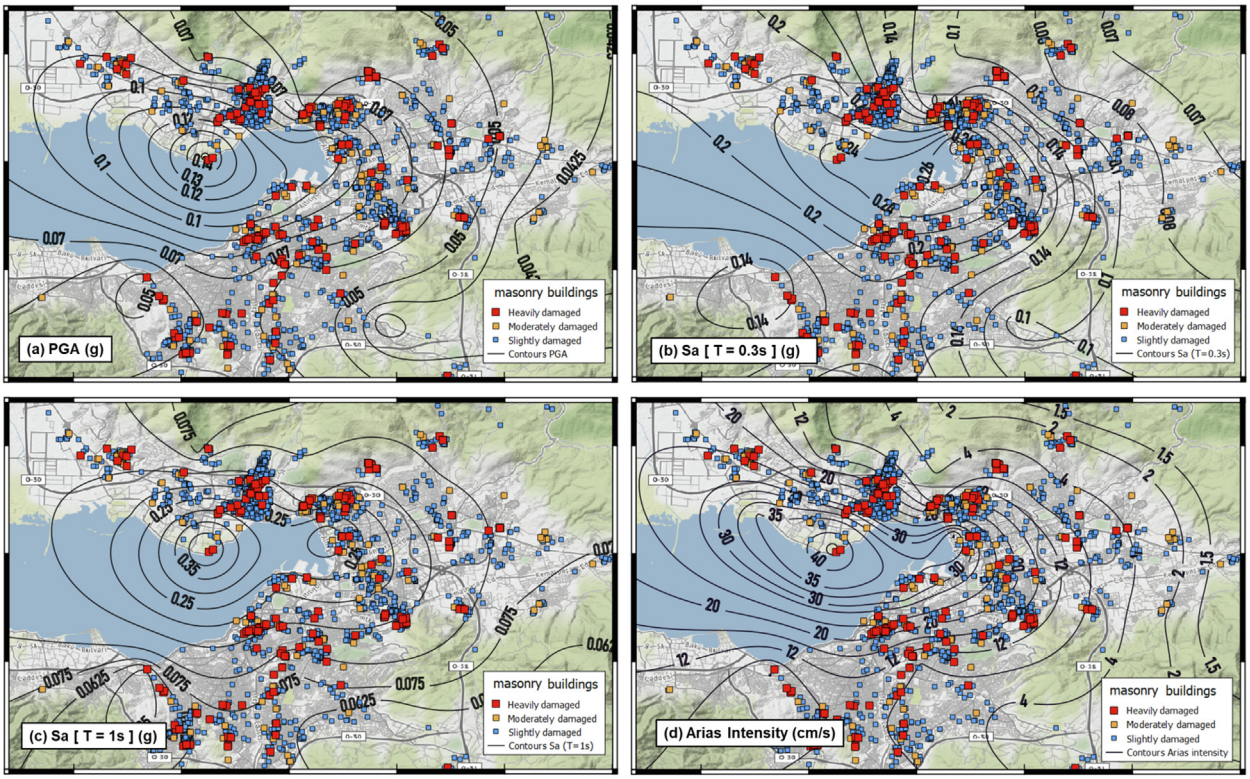

Fig. 11. Distribution of slightly, moderately and heavily damaged masonry buildings correlated with the contours of a) PGA, b) S_a (T = 0.3 s), c) S_a (T = 1 s) and d) Arias Intensity.

construct higher reinforced concrete structures. However, these types of structures can still be encountered throughout Izmir. Damages in masonry structures with a maximum of two stories were encountered in Karşıyaka, Bayraklı, Konak, Bornova, Gaziemir, Buca, Konak, and Karabağlar districts. It is interesting to note that heavy damage was observed in a wide range of PGAs from 0.05 g to 0.14 g. Similarly, the damage is concentrated in Karşıyaka, Bayraklı and Bornova Districts, however, masonry buildings in the old city center to the south seem to be severely affected. It is evident that the damage distribution is in good agreement with the contours, but at the same time, the observed damage is quite widespread highlighting a remarkable role played by the vulnerability of the masonry structures.

Fig. 12 summarizes the distribution of the number of damaged buildings divided into the three previous typologies and the three levels of damage as a function of the distance from the epicenter. These distributions are further compared with the spatial distribution of the ground motion parameters (Arias Intensity, PGA, spectral accelerations at periods 0.3 s and 1 s). The comparison shows that the damage distribution of high-rise buildings (more than 6 stories) can be only roughly approximated as normally distributed around about 75 km (Fig. 12d, h, l). One can observe that there is no collapse outside the Bornova valley of the Izmir Bay region (epicentral distance between 60 and 80 km). This can be related to two reasons: first, there is a small number of high-rise buildings outside the region of Izmir Bay and the second is the change of the frequency contents and the amplification related to the valley effect. For concrete buildings with less than 6 stories, the damages are normally distributed around about 70 km. A lower concentration of damage is observed around 40 km (Fig. 12c, g, k). For masonry buildings, the damages are also almost normally distributed around about 70–75 km. A lower concentration of damage is also observed around distances of 30 and 40 km (Fig. 12b, f, j).

6. Conclusions

Regional scale analysis of the data of the October 30, 2020 event suggests that a complex combination of several factors explains the damages produced in Izmir metropolitan area. The interpretation of the damage pattern is mainly sought in the soft sediments filling the basin and the structure of the basin itself, along with the characteristics of the building stock (significant lack of code compliance).

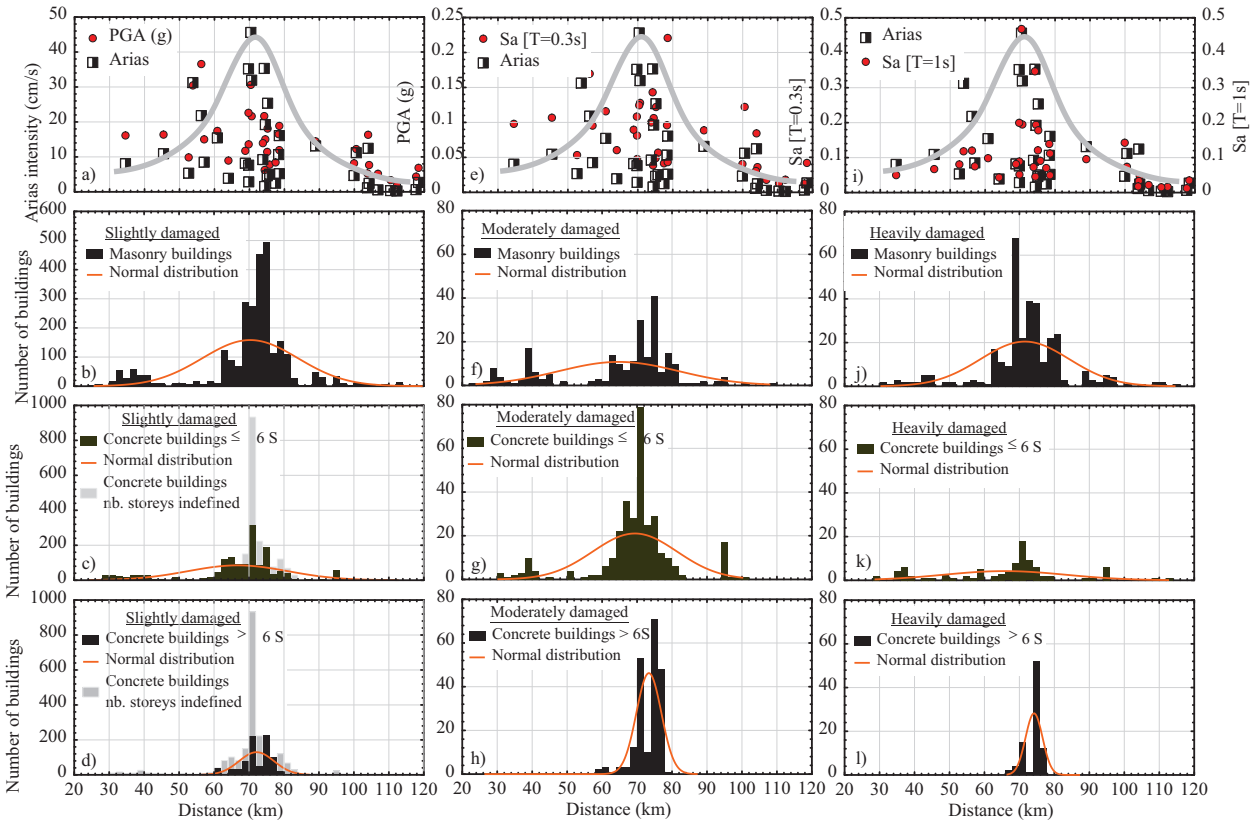

Fig. 12. Distribution of the Arias Intensity (a, e, i), PGA (a) and spectral ordinate for T = 0.3 s (e) and 1 s (i) as a function of the distance; distribution of the damaged buildings as a function of the level of damage (slightly b, c, d, moderately f, g, h and heavily j, k, l damaged) and distance from the epicenter for masonry (b, f, j); concrete structures with less than 6 stories, identified with '≤ 6S' (c, g, k) and concrete structures with more than 6 stories identified with 'greater than 6S' (d, h, l).

Ground motion analysis reveals that a significant amplification is associated not only with the thickness and stiffness of the soil deposits but also with the multiple reflections produced by the basin or valley effects, i.e., an increase in the duration of the seismic event as revealed by the Arias intensity distribution.

Site effects due to the local basin overlap with the main characteristics of this far-field event. The amplitude of the shaking is amplified in the Bornova Plain because of the presence of soft sediments that exhibit a PGA approximately three times higher than the ground motion recorded on the rock (Fig. 4). The shaking coming from the south direction, already rich in low frequencies owing to the long distance from the epicenter, is further modified by the deformability of the basin, because the natural period of the basin is estimated to be approximately 1 s (Pamuk et al., 2019). The resonance between the frequency content of the incoming shaking and the natural period of the basin induced a large plateau in the acceleration response spectra (Fig. 4c) between 0.6 and 1.5 s.

A comparison between the observed damage and mapped parameters of the recorded shaking suggests that the structural performance is below the expected level, possibly because of design and/or construction process deficiencies combined with the number of cycles increased by the multiple reflections.

Analysis of the distribution of damages revealed that the earthquake caused damage all over the boundaries of Izmir province, however, the concentration of moderately and heavily damaged concrete buildings with more than six stories are particularly evident in the basin area highlighting a double resonance effect among ground motion, soil deposits, and high concrete buildings, which reasonably explains the severe damage suffered by such structures.

Future in-depth investigations of the soil properties of the thick alluvial layer in Izmir will further verify the above findings at the scale of single manufacturers, by improving the awareness of the local authorities of the existing seismic risk and contributing to the improvement in understanding the geotechnical factors affecting the site response of similar basins.

Besides, future near-field earthquakes (from the active faults surrounding the city of Izmir) may portend an extremely worrying situation concerning a greater number of fatalities and much more significant damage. As such, retrofit/replacement campaigns are needed to address this risk.

Declaration of Competing Interest

The authors declare that they have no known competing financial interests or personal relationships that could have appeared to influence the work reported in this paper.

Acknowledgements

The contributions of the Ministry of Environment, Urbanisation and Climate Change by providing the characteristics of the built environment; and the graduate students of EGE University involved in the field reconnaissance activities are highly acknowledged.

References

AFAD 2020. Preliminary evaluation report for the Mw=6.6 October 30 2020 Earthquake off the coast (17,26km) of Seferihisar-Aegean Sea (İzmir), Research report (In Turkish).

Akansel, V.H., Özkula, G., 2021. The 30 October 2020, Mw 6.6 Sisam (Samos) earthquake: Interpretation of strong ground motions and post-earthquake condition of nearby structures. Eur. J. Eng. Appl. Sci. 4 (2), 66–89.

Akbaş, B., Akdeniz, N., Aksay, A., Altun, İ.E., Balcı, V., Bilginer, E. et al., 2011. 1:1.250.000 scale Geological Map of Türkiye. General Directorate of Mineral Exploration and Research, Ankara-Türkiye.

Akkar, S., Bommer, J.J., 2010. Empirical equations for the prediction of PGA, PGV and spectral accelerations in Europe, the Mediterranean region and the Middle East. Seismol. Res. Lett. 81, 195–206.

Akkar, S., Çağnan, Z., 2010. A local ground-motion predictive model for Türkiye, and its comparison with other regional and global ground-motion models. Bull. Seismol. Soc. Am. 100 (6), 2978–2995. https://doi.org/10.1785/0120090367.

Altun, S., Sezer, A., Göktepe, A.B., 2012. A preliminary microzonation study on Northern Coasts of Izmir: Investigation of the local soil conditions. Soil Dyn. Earthquake Eng. 39, 37–49.

Ambraseys, N., 2009. Earthquakes in the mediterranean and middle east: A multidisciplinary study of seismicity up to 1900. Cambridge University Press, Cambridge, UK.

Arias, A., 1970. A measure of earthquake intensity. In: Hansen, R.J. (Ed.), Seismic Design for Nuclear Power Plants. MIT Press, Cambridge, MA, pp. 438–483.

Bielak, J., Xu, J., Ghattas, O., 1999. Earthquake ground motion and structural response in alluvial valleys. J. Geotech. Geoenviron. Eng. 125 (5), 413–423. https://doi.org/10.1061/(ASCE)1090-0241(1999)125:5(413).

Boduroglu, H., Ozdemir, P., Binbir, E., Ilki, A., 2013. Seismic damage assessment methodology developed for Turkish Compulsory Insurance System. *9th Annual conference of the international institute of infrastructure renewal and reconstruction*, Brisbane, Australia.

Boore, D.M., Atkinson, G.M., 2008. Ground-motion prediction equations for the average horizontal component of PGA, PGV, and 5%-damped PSA at spectral periods between 0.01 s and 10.0 s. Earthq. Spectra 24, 99–138.

Bradley, B.A., Wotherspoon, L.M., Kaiser, A.E., Cox, B.R., Jeong, S., 2018. Influence of Site Effects on Observed Ground Motions in the Wellington Region from the Mw 7.8 Kaikōura, New Zealand, Earthquake *Bull. Seismol. Soc. Am.*, 108, 3B, 1722–1735, July 2018, doi: 10.1785/0120170286.

CEN 2004. European Committee for Standardisation. Eurocode 8: Design of Structures for Earthquake Resistance. Part 1: General Rules, Seismic Actions and Rules for Buildings, European Standard EN 1998-1: 2004 (stage 51). May 2004.

Çetin, K.Ö., Mylonakis, G., Sextos, A, Stewart, J.P., 2020. Seismological and Engineering Effects of the M 7.0 Samos Island (Aegean Sea) Earthquake, Geotechnical Extreme Events Reconnaissance Association: Report GEER-069 http://dx.doi.org/10.18118/G6H088

Cetin, K.O., Papadimitriou, A.G., Altun, S., et al., 2021. The role of site effects on elevated seismic demands and corollary structural damage during the October 30, 2020, M7.0 Samos Island (Aegean Sea) Earthquake. Bull Earthquake Eng. https://doi.org/10.1007/s10518-021-01265-z.

Cetin, K.O., Altun, S., Askan, A., et al., 2022. The site effects in Izmir Bay of October 30 2020, M7.0 Samos Earthquake. Soil Dyn. Earthquake Eng 152. https://doi.org/10.1016/j.soildyn.2021.107051.

Chiaradonna, A., Monaco, P., Karakan, E., Lanzo, G., Sezer, A., Karray, M. 2022b. Geotechnical Assessment of the Pore Water Pressure Build-

up in Izmir During the October 30, 2020, Samos Earthquake. International Conference on Natural Hazards and Infrastructure, Athens 5-7 July, Code 282299.

Chiaradonna, A., Karakan, E., Lanzo, G., Monaco, P., Sezer, A., Karray, M., 2022a. Influence of local soil conditions on the damage distribution in Izmir bay during the October 30, 2020, Samos Earthquake. Geotech. Geol. Eng. 52. https://doi.org/10.1007/978-3-031-11898-2_62.

Demirci, H.E., Karaman, M., Bhattacharya, S., 2021. A survey of damage observed in Izmir due to 2020 Samos-Izmir earthquake. Nat. Hazards. https://doi.org/10.1007/s11069-021-05085-x.

Erdik, M., Demircioğlu, M.B., Cüneyt, T., 2020. Forensic analysis reveals the causes of building damage in İzmir in the Oct. 30 Aegean Sea earthquake, *Temblor* https://doi.org/10.32858/temblor.139.

Garini, E., Anastasopoulos, I., Gazetas, G., 2020. Soil, basin and soil–building–soil interaction effects on motions of Mexico City during seven earthquakes. *Géotechnique* 70(7), 581-607. ICE Publishing. DOI: 10.1680/jgeot.18.P.314.

Graves, R., 1993. Modeling three-dimensional site response effects in the Marina District Basin, San Francisco, California. *Bull. Seismol. Soc. Am.* 83 (4), 1042–1063. https://doi.org/10.1785/BSSA0830041042.

Guillier, B., Atakan, K., Chatelain, J.L., Havskov, J., Ohrnberger, M., Cara, F., et al., 2008. Influence of instruments on the H/V spectral ratios of ambient vibrations. Bull. Earthquake Eng. 6 (1), 3–31.

Gülerce, Z., Akbaş, B., Özacar, A.A., et al., 2022. Predictive performance of current ground motion models for recorded strong motions in 2020 Samos Earthquake. Soil Dyn. Earthquake Eng. 152. https://doi.org/10.1016/j.soildyn.2021.107053.

Holden, C., Kaiser, A., Van Dissen, R., Jury, R., 2013. Sources, ground motion and structural response characteristics in Wellington of the 2013 Cook Strait earthquakes. Bull. N. Z. Soc. Earthq. Eng. 46 (4), 188–195. https://doi.org/10.5459/bnzsee.46.4.188-195.

Ilki, A., Halici, O., Kupcu, E., Comert, M., Demir, C., 2020. Modifications on seismic damage assessment system of TCIP based on reparability. 17th World Conf. Earthquake Engineering, Sendai, Japan.

Kalogeras, I., Melis, N.S., Kalligeris, N., 2021. The earthquake of October 30th, 2020 at Samos, Eastern Aegean Sea, Greece. Preliminary report of the National Observatory of Athens, Institute of Geodynamics.

Kayan, İ., 2000. Morpho-tectonic units and alluvial geomorphology of the Izmir and its surroundings; Symposium of Earthquake Potential of the Western Anatolia, p.103 (In Turkish).

Kıncal, C., 2005. Engineering Geological Evaluation of the Geological Units Exposed in Inner Bay Area (Izmir)'s Vicinity Using Geographical Information Systems and Remote Sensing, PhD Thesis, p.342, Izmir (In Turkish).

Makra, K., Rovithis, E., Riga, E., Raptakis, D., Pitilakis, K., 2020. *A note on the strong ground motions recorded in Izmir (Turkey) during the October 30 th , 2020 M 7.0 Aegean Sea earthquake: The role of basin effects*. DOI: 10.13140/RG.2.2.34517.65762.

Makra, K., Rovithis, E., Riga, E., Raptakis, D., Pitilakis, K., 2021. Amplification features and observed damages in İzmir (Turkey) due to 2020 Samos (Aegean Sea) earthquake: identifying basin effects and design requirements. Bull. Earthquake Eng. 19 (12), 4773–4804. https://doi.org/10.1007/s10518-021-01148-3.

McGann, C.R., Bradley, B., Wotherspoon, L., Lee, R., 2021. Basin effects and limitations of 1D site response analysis from 2D numerical models of the Thorndon basin. Bull. N. Z. Soc. Earthq. Eng. 54 (1), 21–30. https://doi.org/10.5459/bnzsee.54.1.21-30.

Ministry of Environment, Urbanisation and Climate Change 2020. Report for October 30, 2020 Mw=6.6 Samos Island Earthquake (Off the Coast of Izmir Seferihisar), Earthquake Report (in Turkish). https://hasarte-spit.csb.gov.tr/brosur/hasar_tespit-sunum.pdf.

Moberg, K., 2015. Seismic hazard of the Izmir region, Turkey, based on a probabilistic seismic hazard assessment and stochastic ground motion simulations. University of Bergen, M.Sc. thesis.

NIST 2012. Soil–structure interaction for building structures. NIST GCR 12-917-21. Technical report of the National Institute of Standards and Technology.

Nuhoğlu, A., Erener, M.F., Hızal, Ç., Kıncal, C., Erdoğan, D.Ş., Özdağ, Ö.C., et al., 2021. A reconnaissance study in Izmir (Bornova Plain) affected by October 30, 2020 Samos earthquake. Int. J. Disaster Risk Reduct. 63. https://doi.org/10.1016/j.ijdrr.2021.102465 102465.

Pamuk, E., Akgün, M., Özdağ, Ö., Gönenç, T., 2017. 2D soil and engineering-seismic bedrock modeling of eastern part of İzmir Inner Bay/Turkey. J. Appl. Geophys. 137. https://doi.org/10.1016/j.jappgeo.2016.12.016.

Pamuk, E., Gönenç, T., Özdağ, Ö., Akgün, M., 2018. 3D bedrock structure of Bornova plain and its surroundings (İzmir/Western Turkey). Pure Appl. Geophys. 175, 1–16. https://doi.org/10.1007/s00024-017-1681-0.

Pamuk, E., Özdağ, Ö.C., Akgün, M., 2019. Soil characterization of Bornova Plain (Izmir, Turkey) and its surroundings using a combined survey of MASW and ReMi methods and Nakamura's (HVSR) technique. Bull. Eng. Geol. Environ. 78, 3023–3035.

Papageorgiou, A.S., Kim, J., 1991. Study of the propagation and amplification of seismic waves in Caracas Valley with reference to the 29 July 1967 earthquake: SH waves. Bull. Seismol. Soc. Am. 81 (6), 2214–2233. https://doi.org/10.1785/BSSA0810062214.

Resendiz, D., Roesset, J.M., 1986. Soil–structure interaction in Mexico City during the 1985 earthquake. In The Mexico earthquakes – 1985. Factors involved and lessons learned (eds M. A. Cassaro and E. M. Romero), pp. 193–203.

Seed, H.B., Whitman, R.V., Dezfulian, H., Dobry, R., Idriss, I.M., 1972. Soil conditions and building damage in 1967 Caracas earthquake. J. Soil Mech. Found. 98 (8), 787–806.

Seed, H.B., Romo, M.P., Sun, J.I., Jaime, A., Lysmer, J., 1988. The Mexico Earthquake of September 19, 1985—Relationships between soil conditions and Earthquake ground motions. Earthq. Spectra 4 (4), 687–729. https://doi.org/10.1193/1.1585498.

Sezer, A., Altun S., and Goktepe, A.B. 2008. Microzonation of liquefaction susceptibility in Northern Izmir. *International Conference of Development of Urban Areas and Geotechnical Engineering*, Saint Petersburg, Russia, 16-19 June, pp. 455-460.

Stephenson, W.R., Benites, R., Davenport, P.N., 2009. Localised coherent response of the La Molina basin (Lima, Peru) to earthquakes, and future approaches suggested by Parkway basin (New Zealand) experience. Soil Dyn. Earthquake Eng. 29, 1347–1357. https://doi.org/10.1016/j.soildyn.2009.05.002.

TBEC 2018. Turkish building earthquake code. T.C. Resmi Gazete, Ankara, Turkey.

TSDC 2007. Turkish seismic design code, T.C. Resmi Gazete, Ankara, Turkey.

Yakut, A., Sucuoğlu, H., Binici, B., Canbay, E., Donmez, C., İlki, A., et al., 2021. Performance of structures in İzmir after the Samos Island earthquake. Bull. Earthquake Eng. 1–26. https://doi.org/10.1007/s10518-021-01226-6.

Yegian, M.K., Ghahraman, V.G., Gazetas, G., 1994. Ground-motion and soil-response analyses for Leninakan, 1988 Armenia earthquake. J. Geotech. Eng. 120, 2. https://doi.org/10.1061/(ASCE)0733-9410(1994)120:2(330).

Zhang, B., Papageorgiou, A., 1996. Simulation of the response of the Marina District Basin, San Francisco, California, to the 1989 Loma Prieta earthquake. *Bull. Seismol. Soc. Am.*, 86.

Ziotopoulou, K., Cetin, K.O., Pelekis, P. et al. 2022. Geotechnical reconnaissance findings of the October 30 2020, Mw7.0 Samos Island (Aegean Sea) earthquake. *Bull Earthquake Eng*. https://doi.org/10.1007/s10518-022-01520-x.